

Event-based Motion Segmentation with Spatio-Temporal Graph Cuts

Yi Zhou¹, Guillermo Gallego², Xiuyuan Lu¹, Siqi Liu¹, and Shaojie Shen¹

¹Depts. Electronic and Computer Engineering, Hong Kong University of Science and Technology

²Dept. EECS Technische Universität Berlin and Einstein Center Digital Future, Berlin, Germany

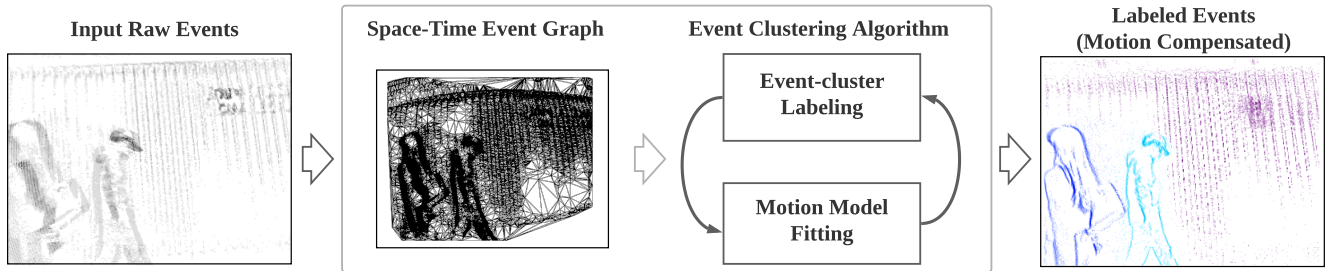


Figure 1: The proposed method clusters the events acquired by an event-based camera (Left: events collapsed along time) into different groups that undergo independent motions (Right). We create a space-time event graph (Middle left), and pass it to an iterative clustering algorithm (Middle right) that jointly classifies events into objects and fits motion models to them. The method (Middle block) fits the event data globally while encouraging spatial coherence and fewest number of clusters.

Abstract

Identifying independently moving objects is an essential task for dynamic scene understanding. However, traditional cameras used in dynamic scenes may suffer from motion blur or exposure artifacts due to their sampling principle. By contrast, event-based cameras are novel bio-inspired sensors that offer advantages to overcome such limitations. They report pixel-wise intensity changes asynchronously, which enables them to acquire visual information at exactly the same rate as the scene dynamics. We have developed a method to identify independently moving objects acquired with an event-based camera, i.e., to solve the event-based motion segmentation problem. This paper describes how to formulate the problem as a weakly-constrained multi-model fitting one via energy minimization, and how to jointly solve its two subproblems –event-cluster assignment (labeling) and motion model fitting– in an iterative manner, by exploiting the spatio-temporal structure of input events in the form of a space-time graph. Experiments on available datasets demonstrate the versatility of the method in scenes with different motion patterns and number of moving objects. The evaluation shows that the method performs on par or better than the state of the art without having to predetermine the number of expected moving objects.

1. Introduction

Dynamic scene understanding is a paramount topic because it enables synthetic agents to interact with their environment better than if they assumed the world was static. Among the many challenges posed by dynamic scenes, we consider the problem of multi-motion segmentation, which consists of detecting and modeling independently moving objects (IMOs) while estimating the camera’s ego-motion. The main difficulty lies in the fact that, without prior knowledge about the scene, the problem is exploratory by nature: multiple hypotheses about both background and IMOs need to be considered and checked against the data to select the best fit. Additionally, from an application perspective, challenging visual effects, such as motion blur (induced by fast motions) and over/under-exposure imaging (in challenging illumination conditions) make the problem even harder for pipelines based on standard cameras.

Event-based cameras, such as the Dynamic Vision Sensor (DVS) [1], are novel bio-inspired visual sensors. Unlike standard cameras that capture at a fixed frame rate, event-based cameras report per-pixel intensity changes asynchronously at the time they occur, with microsecond resolution, called “events”. This working principle offers potential advantages (low latency, high temporal resolution, high

dynamic range and low power consumption) to tackle challenging scenarios in computer vision such as high-speed and/or high dynamic range (HDR) feature tracking [2, 3, 4], camera tracking [5, 6, 7], control [8, 9] and Simultaneous Localization and Mapping (SLAM) [10, 11, 12, 13]. However, due to the above principle of operation and unconventional output, algorithms designed for standard cameras cannot be directly applied. Novel algorithms are needed to unlock event cameras’ potentials. The recent paper [14] provides a comprehensive review on event-based cameras, algorithms and applications.

In this paper, we consider the problem of event-based motion segmentation, which aims at clustering events occurred during a time interval into several groups that represent coherent moving objects. We tackle the most general case: a possibly moving event camera observing a dynamic scene. It is more challenging than the static camera case because events are no longer solely due to the IMOs; they are also induced by the background. We develop a method to jointly cluster the events and estimate their coherent motion, in an iterative and alternating manner.

Contribution. Our contribution can be summarized as:

1. A novel event-based motion segmentation method designed in the spirit of motion compensation [15] and built on top of classical multi-model fitting schemes. We propose a space-time event graph to exploit the spatio-temporal nature of events, leading to globally consistent and locally coherent labeling results.
2. A simple and effective initialization method using the original motion compensation scheme on raw events.
3. A formulation that does not require prior knowledge in the form of scene geometry, motion patterns or number of IMOs.
4. An extensive evaluation on available datasets, showing on par or better performance than the state of the art.

In the following sections we review related work (Section 2), present our approach (Sections 3 to 5) and evaluate its performance on actual data (Section 6).

2. Related Work

Early works on event-based motion segmentation required prior knowledge on either the shape of IMOs (*e.g.*, a circle [16]) or the correlation between the tracked geometric primitives and the motion of the event camera [17]. Such prior knowledge is no longer required in recent works [18, 19, 20, 21, 22]. Several of these pipelines follow a greedy strategy, which consists of analyzing the dominant events (*e.g.*, background), then removing these (by empirical thresholding [18, 19]) and analyzing the remaining events (*i.e.*, the IMOs), greedily.

Using the method of [19] as initialization, [20] was the first one to solve the model-fitting and event-object associ-

ation (labeling) problems jointly. By leveraging the idea of motion compensation [15], it formulated the segmentation problem using an expectation-maximization (EM) scheme, which iteratively updated the soft data associations (event-cluster assignments) and motion model parameters. It provided per-event segmentation rather than classical bounding-box results. More recently, [21] proposed a similar joint optimization method, but with differences: (*i*) initialization of IMO clusters was based on K-means clustering of event-based feature tracks; (*ii*) event-cluster assignments were based on morphological operations via empirical thresholding. In addition to the above methods, [22] proposed a supervised end-to-end learning-based pipeline that simultaneously solved for optical flow, 3D motion and object segmentation. Although [22] is not closely related to the above approaches (neither is to ours), it provides a state-of-the-art dataset for evaluation of IMOs segmentation.

Like previous methods (*e.g.*, [20]), our method also allows general parametric warps (motion models) and performs per-event segmentation. Besides, we are also able to produce sharp, motion-compensated images as a by-product (Fig. 1, Right). However, we claim the following fundamental differences compared to previous approaches. First, the problem is formulated as a Markov Random Field (MRF) problem by exploiting the spatio-temporal nature of events, thus, can be efficiently solved with graph-cut algorithms. Second, we pose the problem as a joint optimization over the motion parameters and event associations, but contrary to [20] we introduce spatial regularizers. In particular, we explicitly minimize the number of clusters and smooth their shape, which is pursued naturally via a penalty/energy formulation. Third, we also leverage the event alignment for event classification into clusters, but we propose a novel formulation using negated Images of Warped Events (IWEs). Finally, we do not follow the greedy strategy nor do we need additional methods for initialization (*e.g.*, feature tracking [21]). We provide a new initialization method, based on a hierarchical subdivision of the volume of events to provide a pool of motion instances.

3. Problem Statement Preliminaries

The goal of this work is to cluster the events produced by an event-based camera into groups that undergo coherent motions. Such motions aim to represent the unknown number of IMOs in the scene. Once clustered, events are warped according to the estimated motions and produce an overall IWE with the highest contrast (Fig 1, Right).

In this section we briefly introduce multi-model fitting and discuss how to adapt its components to event data. We introduce the notions of spatio-temporal graph of events and model-fitting metric(s) on the graph.

3.1. Multi-Model Fitting

Multi-model fitting is a category of computer vision problems that aim at explaining data using several model instances. It is a chicken-and-egg problem, often split into two sub-problems: assignment of data to a model instance (i.e., labeling) and model fitting (i.e., parameter estimation). Examples consist of recognizing and segmenting partially occluded objects in 2D [23] or 3D [24], optical flow estimation [25, 26, 27], and motion segmentation [28]. These problems aim at assigning a label l_p to each data point p , where each label $l \in \mathcal{L}$ corresponds to a model \mathcal{M}_l that is consistent with local observations. The solution to the problem is a labeling configuration L that is locally smooth and globally consistent. To find such a solution, multi-model fitting problems are naturally formulated as the minimization of an energy $E = E_{\text{data}} + E_{\text{reg}}$, comprising a data term E_{data} that measures the inconsistency between the data and the models, and a regularizer (smoothness term) E_{reg} that enforces prior knowledge about the models. A successful set of solvers consider a graph through the data points and seek to partition the graph into the optimal labels [29]. We also follow this approach.

3.2. Space-Time Event Graph

The data points in our problem consist of events produced by a DVS [1]. An event $e_k = (\mathbf{x}_k, t_k, p_k)$ represents the intensity change of a predefined size C that occurs at pixel \mathbf{x}_k and time t_k , with sign $p_k \in \{-1, +1\}$ (intensity decrease or increase). Because events are sparse in the spatio-temporal domain (time-evolving image plane), the underlying graph considered is in general unstructured (as opposed to the regular graph of pixel intensities in an image). To build a spatio-temporal graph for events while keeping a low complexity, we propose to use a Delaunay triangulation [30] on the binary image of active events in the space-time volume \mathbf{V} (Fig. 2).

Specifically, given the events in a volume \mathbf{V} of size $W \times H \times \delta t$ (where W, H refer to the width and height of the image plane, and δt denotes the time span), we first compute a binary image of event activity (i.e., the pixel is 1 if it contains at least one event, and it is 0 otherwise). Then we compute the Delaunay triangulation on the non-zero pixels of this binary image (black dots in Fig. 2), which returns a 2D graph (mesh). This 2D graph is used to build a space-time (3D) graph for the events (see Fig. 2). Each event typically has $2 + 2N$ neighbors in the resulting graph, where N denotes the number of edges that link to the event’s pixel location in the binary image (black dots in Fig. 2).

There are many possible graphs that can be used to connect the event data points. The above proposal is inspired in graphs proposed for Markov Random Fields built on sets of sparse 2D features [31] and is easy to implement from a data structure point of view.

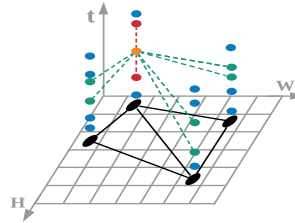


Figure 2: Spatio-temporal graph of events, with each event (orange dot) connected to its two temporally-closest (i.e., past and future) events at the same pixel (red dots) and to the neighbouring pixels (green dots) in the Delaunay triangulation built from the active pixels (black dots).

3.3. Goodness of Fit by Motion Compensation

The specification of a metric on the data graph allows us to assess the goodness of fit between the data and the model(s) (i.e., E_{data}). Building upon [32], the goodness of fit is given by the alignment of the events along point trajectories on the image plane, which constitute a motion model and are parametrized by a parameter vector \mathbf{m} . Such event alignment is assessed by the strength of the contours of an IWE. The contour strength (which is related to image contrast [33]) can be measured with various dispersion metrics, such as variance [34, 15, 20], RMS of mean timestamp per pixel [18, 22, 21], etc. We utilize the variance loss as metric for the edges of the event graph. To make the paper self-contained, we briefly review the idea of motion compensation [34, 15], upon which motion models are fitted.

Motion Model Fitting. The contrast maximization framework [15] allows us to fit a motion model to a group of events $\mathcal{E} = \{e_k\}_{k=1}^{N_e}$. First, events are geometrically transformed according to a warping function \mathbf{W} ,

$$e_k \doteq (\mathbf{x}_k, t_k) \mapsto e'_k \doteq (\mathbf{x}'_k, t_{\text{ref}}), \quad (1)$$

leading to a set of warped events $\mathcal{E}' = \{e'_k\}_{k=1}^{N_e}$ at a reference time t_{ref} . The warping function $\mathbf{W}(\mathbf{x}_k, t_k; \mathbf{m}) \doteq \mathbf{x}'_k$ implements the image-plane trajectories of a motion model and is parametrized by \mathbf{m} . Secondly, events \mathcal{E}' are aggregated into an image (or histogram) of warped events (IWE),

$$I(\mathbf{x}; \mathbf{m}) \doteq \sum_{k=1}^{N_e} \delta(\mathbf{x} - \mathbf{x}'_k(\mathbf{m})), \quad (2)$$

where each pixel \mathbf{x} counts the number of warped events that fall within it. In practice, the Dirac function δ is replaced by a Gaussian $\mathcal{N}(\mathbf{x}; \mathbf{0}, \epsilon^2 \text{Id})$ of $\epsilon = 1$ pixel width. Finally, the variance of the IWE defines a criterion for model fitting: $\mathbf{m}^* = \arg \max_{\mathbf{m}} \sigma^2(I(\mathbf{x}; \mathbf{m}))$. Like [15], our formulation supports any type of parametric motion model, such as 2-DoF flow [3], 3-DoF rotational motion [34], 4-DoF model [18], etc.

In summary, the above event graph representation and model fitting criterion allow us to formulate the problem of event-based multi-motion segmentation as joint estimation over two sets of variables:

- **Discrete labels.** The segmentation (clustering) is represented by the labeling function $L(e) : \Omega \times \mathcal{T} \rightarrow \mathcal{L} = \{1, \dots, N\}$, which assigns to each event e a label $l \in \mathcal{L}$ indicating which independently moving object the event belongs to.
- **Motion models.** The motion of the independently moving object is represented by a collection of warps with parameters $\mathcal{M} = \{\mathbf{m}_1, \dots, \mathbf{m}_N\}$. Each warp represents the coherent motion of a group of events.

4. Designed Energy for Motion Segmentation

We propose an energy function that considers jointly the sub-problems of labeling (i.e., segmentation) and model fitting. The energy function is defined on both unknowns (labeling configuration L and cluster motions \mathcal{M}) as

$$E(L, \mathcal{M}) \doteq E_D(L, \mathcal{M}) + \lambda_P E_P(L) + \lambda_M E_M(L), \quad (3)$$

where E_D denotes the data term and E_P, E_M constitute the regularizer. Specifically, E_P is the regularizer of the Potts functional [35] and E_M is a label cost term representing the Minimum Descriptor Length (MDL) principle [36]. The weights $\lambda \geq 0$ balance the contribution of each term.

The energy is designed such that its minimizer achieves the best fit to the data while being spatio-temporally smooth and having the fewest labels (i.e., segments). We detail the design of each energy term in the upcoming sections.

4.1. Data Fidelity Term

The data term in (3) is defined on both the discrete labeling variables and the continuous model parameters. If the labeling variables are fixed, the energy reduces to the data term and the optimal motion model for each cluster can be obtained using the motion compensation scheme (see Section 5.2). Hence, we focus on the design of the data term from the perspective of the discrete labeling variables.

To adapt motion compensation [15] to a graph-based energy formulation (3) we need to reformulate it so that: (i) energy is minimized instead of maximized, (ii) the fitting cost of a group of events is given by the sum of fitting costs of individual events, i.e., the so-called unary terms [29].

The original motion compensation scheme creates an IWE (2), on which image contrast is measured. The IWE is created by warping events according to a certain motion model. The higher the IWE contrast, the sharper the IWE, and consequently, higher pixel values (i.e., event accumulation) appear around the edge patterns. Therefore, the intensity value at each IWE pixel is a proxy for the consistency (goodness of fit) between the model and the events that are

warped to that pixel. To convert the maximization problem into a minimization one and to build the unary costs of the data term, we propose the idea of IWE “negative”. Once an IWE I is computed (2), it is normalized to a fixed range, e.g., $[0, 255]$, and then its negative is calculated as $\bar{I} = 255 - \hat{I}$, where $\hat{\cdot}$ denotes the normalization operation, and $\bar{\cdot}$ the negative operation. We define the unary term for an event e_k as the value at its warped location, \mathbf{x}'_k in (1), on the IWE negative, namely $\bar{I}(\mathbf{x}'_k; \mathbf{m}_l)$. The data term is defined as the sum of all unary terms:

$$E_D(L) \doteq \sum_{l \in \mathcal{L}} \sum_{e_k \in \mathcal{C}_l} \bar{I}(\mathbf{x}'_k; \mathbf{m}_l), \quad (4)$$

where \mathcal{C}_l denotes the cluster of events with label l , and $\bar{I}(\cdot; \mathbf{m}_l)$ the IWE negative created using motion model \mathbf{m}_l .

4.2. Spatially Coherent Labeling

As for the regularizer, we simply use a pairwise Potts model term E_P to encourage spatially coherent labeling. This term is defined only on the discrete labeling variables:

$$E_P(L) \doteq \sum_{e_i, e_j \in \mathcal{N}} \delta_{L(e_i), L(e_j)}, \quad (5)$$

where \mathcal{N} denotes the event neighbourhood in the spatio-temporal graph (Section 3.2), and $\delta_{m,n}$ is the Kronecker delta (1 if the variables m, n are equal, and 0 otherwise).

4.3. Encouraging Few Number of Segments

To discourage redundancy of the assigned motion models we introduce an MDL term:

$$E_M(L) \doteq \sum_{l=1}^N \psi(l), \quad \psi(l) \doteq \begin{cases} 1 & \text{if } \sum_{e \in \mathcal{C}_l} \delta_{L(e), l} > 0 \\ 0 & \text{otherwise.} \end{cases} \quad (6)$$

This term penalizes the total number of assigned (active) labels (i.e., segments), which encourages it to converge to the actual number of IMOs.

We describe the optimization procedure for solving the proposed energy in the next section.

5. Joint Optimization of Motions and Segments

We now discuss how to minimize the proposed energy function (3). This energy depends on both discrete labeling variables L and continuous motion parameters \mathcal{M} , thus leading to a discrete-continuous optimization problem. Following the efficient solvers used in classical multi-model fitting methods [36, 27], we employ a block-coordinate descent strategy to optimize L and \mathcal{M} in an alternating manner. We present the solution to each sub problem, followed by the initialization strategy. The overall method is summarized in Algorithm 1.

Algorithm 1 Event-based motion segmentation by discrete-continuous optimization.

- 1: *Input*: \mathcal{E} events in a space-time volume.
 - 2: *Output*: event cluster assignments (i.e., labels L) and fitted motion per cluster (\mathcal{M}).
 - 3: Initialize \mathcal{M} , L (Section 5.3).
 - 4: Create event graph (Section 3.2).
 - 5: **Iterate** until convergence:
 - 6: Fix \mathcal{M} , update L (Section 5.1, graph cut).
 - 7: Fix L , update \mathcal{M} (Section 5.2).
-

5.1. Segmentation: update labels L given motions \mathcal{M}

The overall energy (3) reduces to the sub-problem of discrete labeling when motion models \mathcal{M} are fixed:

$$E(L) = E_D(L) + \lambda_P E_P(L) + \lambda_M E_M(L). \quad (7)$$

This energy describes a standard MRF problem plus an additional MDL term. To minimize (7), we apply the α -expansion based graph-cut method [29] combined with the method in [36] to handle the label costs induced by the MDL term. To accelerate the algorithm, if a motion model is not assigned to any cluster of events, it is removed from the model pool. The remaining models (label ID) are sorted according to the number of events that belong to the corresponding clusters.

5.2. Model Fitting: update motions \mathcal{M} given labels L

When the label variables are fixed, the energy (3) simplifies to the data term only. The continuous variables of each motion model can be re-fitted independently from other motion models using the corresponding cluster of events. The original motion compensation scheme (Section 3.3, [15]) is applied for model fitting.

5.3. Initialization

Let us show how to initialize the optimization procedure. Unlike other solvers, which greedily initialize motion models \mathcal{M} by clustering optical flow [19] or feature tracks [21], we propose a simple and effective hierarchical initialization based on the original motion compensation scheme.

Given a space-time volume \mathbf{V} of events \mathcal{E} , we carry out an N -level subdivision operation. At level $n \in [0, N - 1]$ of the hierarchy, the volume \mathbf{V} is divided evenly into 4^n sub-volumes. Let us use $N = 4$ as an example, as shown in Fig. 3, where the blue dashed rectangle illustrates a sub-volume at level $n = 1$, while the green one shows a sub-volume at level $n = 3$. For simplicity, the volume \mathbf{V} is visualized in 2D, namely by accumulating events on the reference time slice. After the division operations, we have $4^0 + 4^1 + \dots + 4^3 = 85$ sub-volumes (including the whole volume at the base level of the hierarchy). By feeding the

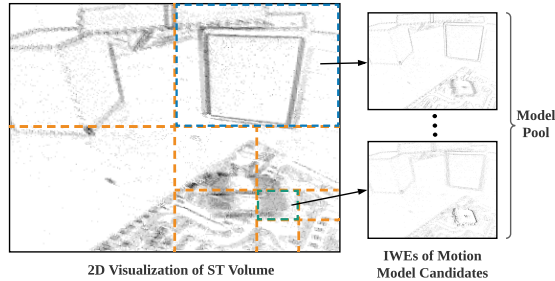


Figure 3: Initialization of motion model candidates. The division operation is illustrated by the orange dashed buckets. The model pool consists of all IWEs (negative) created using the corresponding model candidates.

events in these sub-volumes to the motion compensation scheme, we get a pool of 85 motion model candidates \mathcal{M} .

This strategy aims at capturing IMOs of different size. As illustrated in Fig. 3, the blue dashed sub-volume captures one of the boxes in the background, which leads to an IWE with high contrast at the background structures, whereas the green dashed sub-volume senses part of a smaller IMO, which leads to an IWE with high contrast around that IMO. The resulting model pool is used in the computation of the data term (Section 4.1).

6. Experiments

In this section we evaluate the proposed algorithm. First, we present the datasets and evaluation metrics used (Section 6.1). Second, we provide both quantitative and qualitative results on several datasets and compare against state-of-the-art baselines (Section 6.2). Third, justify how the parameters are chosen (Section 6.3). Finally, we analyze the computational efficiency of our implementation (Section 6.4) and discuss its limitations (Section 6.5).

6.1. Datasets and Evaluation Metrics

We evaluate Algorithm 1 extensively on datasets accompanying recent publications [18, 20, 22, 37]:

- The Extreme Event Dataset (EED) [18] is one of the first open-source datasets used for the research of IMO detection and tracking. Besides the camera’s ego motion, there are other IMOs (up to three) in each sequence. It provides manually-annotated bounding boxes for quantitative evaluation. All sequences are collected in a laboratory environment, aiming to demonstrate the outstanding performance of event cameras in HDR scenarios.
- EVIMO [22] is also collected in a lab environment but with better illumination. Up to three IMOs appear in the sequences. For evaluation, it provides dense segmentation masks of the IMOs.

Table 1: Summary of characteristics of the datasets used.

Dataset	Sensor Type	Sensor Status	#IMO	Env.	HDR
EED [18]	DAVIS240	Moving	1-3	Indoor	Yes
EVIMO [22]	DAVIS346	Moving	1-3	Indoor	No
EMSMC [20]	DAVIS240	Moving	1- N	Outdoor	Yes
DistSurf [37]	DAVIS346	Static	1- N	Indoor	No

- EMSMC [20] provides a set of real-world sequences captured in both indoor and outdoor environments. Different from the above two datasets, it consists of a larger number of IMOs and even with non-rigid motions. HDR scenarios are also captured in this dataset.
- DistSurf [37] is a dataset collected specifically for evaluating event-based optical flow estimation. We find the data is in good quality and can be used for qualitative evaluation of our algorithm.

Table 1 summarizes the key characteristics of the datasets.

Evaluation Metrics. For quantitative evaluation we use two standard metrics. The first one is *detection rate* based on the overlap between the bounding boxes of detected and labeled objects, which was introduced in [18] and used ever since. It considers the detection results as successful if it meets the following conditions: $\mathcal{B}_D \cap \mathcal{B}_G > 0.5$ and $(\mathcal{B}_D \cap \mathcal{B}_G) > (\mathcal{B}_D \cap \overline{\mathcal{B}_G})$, where \mathcal{B}_D refers to the estimated bounding box (or convex hull), \mathcal{B}_G the ground truth bounding box, and $\bar{\cdot}$ denotes the complement of a set.

The second metric is *Intersection over Union* (IoU), which is the most commonly used metric to evaluate the performance of segmentation methods, and was proposed for event data in [21, 22]. IoU is typically formulated as $\text{IoU} = (\mathcal{S}_D \cap \mathcal{S}_G) / (\mathcal{S}_D \cup \mathcal{S}_G)$, where \mathcal{S}_D refers to the resulting segmentation mask and \mathcal{S}_G the ground truth mask. Note that the result of our algorithm consist of sparse warped events with specific labels. To obtain a dense segmentation mask from a cluster of warped events, we label all pixels in its convex hull identically.

6.2. Quantitative and Qualitative Evaluation

EED Dataset. We first evaluate our algorithm on the EED [18] dataset using the detection rate metric. Seen from the quantitative results in Table 2, our algorithm outperforms other state-of-the-art solutions [18, 20, 21] in terms of average detection rate. The numbers for the baseline methods are taken from the corresponding publication. Qualitative results are given in Fig. 4, where the red rectangles are ground truth bounding boxes.

EVIMO Dataset. A second quantitative evaluation is performed on the EVIMO dataset using the IoU metric. As shown in Table 3, our algorithm performs the second best (0.19% lower than the best one) among all four segmentation methods. The numbers for the baseline methods are

Table 2: Comparison with state-of-the-art methods using detection rate (proposed by [18]) of independently moving objects (in %).

EED sequence	SOFAS [19]	EED [18]	EMSMC [20]	MOMS-E [21]	Ours (Alg. 1)
Fast drone	88.89	92.78	96.30	-	96.30
Lighting variation	0.00	84.52	80.51	-	100.00
Occlusions	80.00	90.83	92.31	-	90.91
What is background?	22.08	89.21	100.00	-	100.00
Average	47.74	89.34	92.28	94.20	96.80

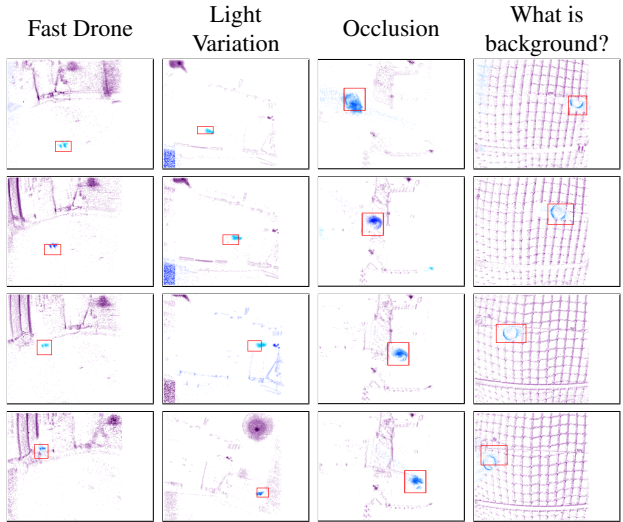


Figure 4: Segmentation results on EED dataset [18]. Time runs from top to bottom. The ground truth bounding boxes (in red) show the 2D location of the IMOs. Note that such boxes are manually annotated on the DAVIS grayscale images, which are not perfectly time-aligned with the events. Hence, offsets are witnessed for fast-moving IMOs.

taken from [21]. During the experiment, we found several issues that may deteriorate the IoU score. First, the ground truth masks are not perfectly aligned with objects in the raw images because of inaccurate CAD models and 6-DoF IMO poses produced by the motion capture system. Second, our labeled IWE and segmentation masks are computed using undistorted events (using camera calibration); then the masks are warped to the raw (distorted) image plane where the IoU score is calculated. Undistortion leads to information loss near image boundaries. Third, we found that some of the IMOs are hanged by the person who was holding the event camera, thus, the IMOs sometimes undergo the same motion as the camera. In such a case, IMOs are labeled as background motion and no IoU score is calculated.

Exemplary results are given in Fig. 5, where both labeled IWEs and their corresponding dense segmentation masks are visualized. In the box sequence, the toy car traverses

Table 3: Comparison with state-of-the-art methods on the EVIMO dataset [22] using the IoU metric (in %).

Method	EVIMO [22]	EVDodgeNet [38]	MOMS-E [21]	Ours
IoU	77.00	65.76	74.82	76.81

from right to left and can be continuously detected as a moving object. There are two IMOs in the table sequence – a toy car and a top plane. The two move against each other and meet in the middle. They are successfully detected even when they are partially overlapped. The toy plane stays almost still at the end of the sequence, which explains why it is labeled as background. The IWE around the area of the plane looks as sharp as the background, which also indicates that the plane stays still.

EMSMC and DistSurf Datasets. Besides above quantitative results, we also provide an extensive qualitative evaluation on real-world data from EMSMC [20] and DistSurf [37] datasets. These sequences cover a wide variety of scenes, ranging from indoor lab environments to outdoor traffic scenes with moving vehicles and pedestrians, including non-rigid motion and HDR scenarios. We provide exemplary results in Fig. 6. The first column shows a traffic scene captured from above, with three vehicles driving on the road. The two cars moving to the left are in very similar velocity, thus, they are clustered in the same group. Note that the color of each cluster may change from one segmentation to the next. This is a visualization issue due to the fact that clusters are sorted according to the number of events they contain and color is assigned based on this order (we do not perform tracking to achieve color coherence).

The second column of Fig. 6 shows an outdoor HDR scene captured with the event camera facing the sun while a pedestrian and a skateboarder pass by. Our algorithm preserves the motion discrepancy among different parts of the non-rigid human bodies while maintaining the compactness of the segmentation due to the applied MDL term. The third column shows a vehicle passing by in front of buildings. Our algorithm successfully distinguishes the car from the buildings in the background, which are compactly labeled together, thus identifying the pan camera motion. The fourth column shows a fan (whose blades rotate at $\approx 1800^\circ/\text{s}$) and a free-falling coin, *i.e.*, a high-speed scenario. Since our algorithm supports multiple motion models, the fan blades and the coin are successfully detected and distinguished. The fifth column shows a traffic scene captured at street level. The motions of overlapping vehicles can be successfully distinguished. The last column shows a scene with a pair of waving hands. The motions of the hand and arm are sometimes segmented from each other when there is a small wrist motion.

6.3. Parameters of the Method

Let us mention how the parameters of the method are set. First, we process events in packets (*i.e.*, sliding window fashion). The number of events N_e may be selected based on the scene dynamics or texture [40]. However, we found that $N_e \in [15000, 30000]$ is a sensible choice for sequences captured by the DAVIS240 or DAVIS346 [39]. As shown in the experiments, motion parameters can be assumed to be constant within each sliding window.

Second, we set the weights $\lambda_P = 40$, $\lambda_M = 8,000$. The Potts model weight λ_P is set according to the fact that an event typically has at least six spatio-temporal neighbours (At least two edges are linking to the event’s pixel location due to the Delaunay triangulation). The maximum discrepancy for an unary term is 255 according to the IWE negative. Thus, $\lambda_P = 255/6 \approx 40$ so that local consistency would be sacrificed for spatial coherence. The MDL weight λ_M is set empirically. For sequences with relatively small IMOs traversing a textured background, λ_P has to be reduced to avoid over-smoothing effects.

Finally, the number of hierarchy levels is $N = 4$, which determines the size of the sub-volumes used during initialization. N may be increased to deal with very small IMOs. However, this leads to a bad signal-to-noise ratio (Sec. 6.5).

6.4. Computational Performance

Algorithm 1 consists of three main steps: (i) initialization, (ii) creation of event graph, and (iii) alternating discrete-continuous optimization. The initialization is the most time-consuming step. Using 15,000 events as input and a 4-level subdivision as an example, it takes about 4 s to compute all motion candidates of the model pool. This time is spent on one motion model type; for multi-model proposals, *e.g.*, K types, the computation is K times larger. We apply hyper-threading to speed up the process. The creation of the space-time event graph is efficient, taking 45 ms. The optimization terminates within 3 iterations, and its time is proportional to the size of the motion pool; it takes about 3 s. The discrete-labeling (graph-cut) sub problem takes the majority of the runtime compared to the negligible time spent on continuous model fitting.

6.5. Limitations

A limitation observed during initialization entails the size of the IMOs. Small IMOs, *e.g.*, smaller than 1% of the sensor’s spatial resolution, as in the *multiple objects* sequence of [18], cast signal-to-noise ratio problems during motion proposal generation, thus are unlikely to be properly initialized. This could be resolved by using alternative, more greedy initialization methods, which is the topic of future research. The size of the IMOs in the EVIMO, EMSMC and DistDurf datasets is larger than those in EED, thus detecting IMOs is not an issue in the former datasets.

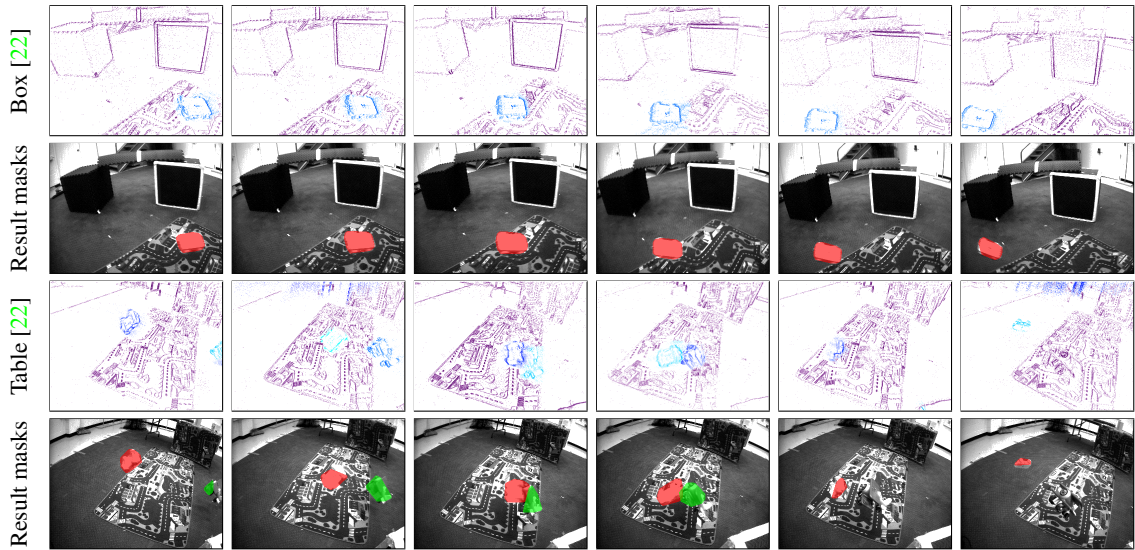


Figure 5: Segmentation results on the EVIMO dataset [22]. Time runs from left to right. The labeled IWEs (rows 1 & 3) are displayed in undistorted coordinates (known camera calibration) while the dense segmentation masks (rows 2 & 4) are shown on the raw (distorted) grayscale images from the DAVIS [39]. Grayscale images are used for visualization only.

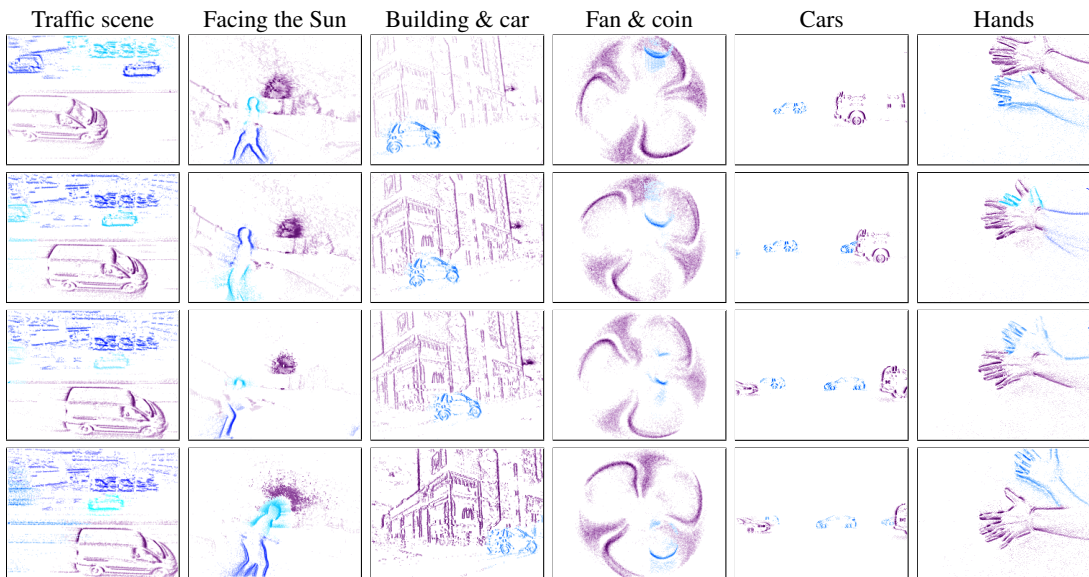


Figure 6: Results on datasets EMSMC [20] (columns 1-4) and DistSurf [37] (columns 5-6). Time runs from top to bottom.

7. Conclusion

We presented a novel method for event-based motion segmentation. Our approach is a multi-model fitting scheme that jointly clusters events and fits motion models to them. The proposed graph-based (MRF) formulation with the additional MDL energy term leads to globally consistent and spatially coherent segmentation results using fewest labels. As a by-product, the method produced labeled, motion-

compensated images of warped events that may be used for further processing (*e.g.*, recognition). A thorough evaluation demonstrated the versatility of our method in scenes with different motion patterns and unknown number of independent motions. We envision that the method could be applied to robotic tasks, *e.g.* navigation or obstacle dodging for autonomous vehicles in difficult (HDR, high-speed) conditions. Moreover, we hope this work inspires new research in applying graph-based techniques to event data.

References

- [1] Patrick Lichtsteiner, Christoph Posch, and Tobi Delbruck, "A 128×128 120 dB 15 μ s latency asynchronous temporal contrast vision sensor," *IEEE J. Solid-State Circuits*, vol. 43, no. 2, pp. 566–576, 2008. 1, 3
- [2] Xavier Lagorce, Cédric Meyer, Sio-Hoi Ieng, David Filliat, and Ryad Benosman, "Asynchronous event-based multikernel algorithm for high-speed visual features tracking," *IEEE Trans. Neural Netw. Learn. Syst.*, vol. 26, pp. 1710–1720, Aug. 2015. 2
- [3] Alex Zihao Zhu, Nikolay Atanasov, and Kostas Daniilidis, "Event-based feature tracking with probabilistic data association," in *IEEE Int. Conf. Robot. Autom. (ICRA)*, pp. 4465–4470, 2017. 2, 3
- [4] Daniel Gehrig, Henri Rebecq, Guillermo Gallego, and Davide Scaramuzza, "EKL: Asynchronous photometric feature tracking using events and frames," *Int. J. Comput. Vis.*, 2019. 2
- [5] Elias Mueggler, Guillermo Gallego, and Davide Scaramuzza, "Continuous-time trajectory estimation for event-based vision sensors," in *Robotics: Science and Systems (RSS)*, 2015. 2
- [6] Guillermo Gallego, Jon E. A. Lund, Elias Mueggler, Henri Rebecq, Tobi Delbruck, and Davide Scaramuzza, "Event-based, 6-DOF camera tracking from photometric depth maps," *IEEE Trans. Pattern Anal. Mach. Intell.*, vol. 40, pp. 2402–2412, Oct. 2018. 2
- [7] William Oswaldo Chamorro Hernandez, Juan Andrade-Cetto, and Joan Solá Ortega, "High-speed event camera tracking," in *British Mach. Vis. Conf. (BMVC)*, 2020. 2
- [8] Jörg Conradt, Matthew Cook, Raphael Berner, Patrick Lichtsteiner, Rodney J. Douglas, and Tobi Delbruck, "A pencil balancing robot using a pair of AER dynamic vision sensors," in *IEEE Int. Symp. Circuits Syst. (ISCAS)*, pp. 781–784, 2009. 2
- [9] Tobi Delbruck and Manuel Lang, "Robotic goalie with 3ms reaction time at 4% CPU load using event-based dynamic vision sensor," *Front. Neurosci.*, vol. 7, p. 223, 2013. 2
- [10] Hanme Kim, Stefan Leutenegger, and Andrew J. Davison, "Real-time 3D reconstruction and 6-DoF tracking with an event camera," in *Eur. Conf. Comput. Vis. (ECCV)*, pp. 349–364, 2016. 2
- [11] Henri Rebecq, Timo Horstschäfer, Guillermo Gallego, and Davide Scaramuzza, "EVO: A geometric approach to event-based 6-DOF parallel tracking and mapping in real-time," *IEEE Robot. Autom. Lett.*, vol. 2, no. 2, pp. 593–600, 2017. 2
- [12] Antoni Rosinol Vidal, Henri Rebecq, Timo Horstschäfer, and Davide Scaramuzza, "Ultimate SLAM? combining events, images, and IMU for robust visual SLAM in HDR and high speed scenarios," *IEEE Robot. Autom. Lett.*, vol. 3, pp. 994–1001, Apr. 2018. 2
- [13] Elias Mueggler, Guillermo Gallego, Henri Rebecq, and Davide Scaramuzza, "Continuous-time visual-inertial odometry for event cameras," *IEEE Trans. Robot.*, vol. 34, pp. 1425–1440, Dec. 2018. 2
- [14] Guillermo Gallego, Tobi Delbruck, Garrick Orchard, Chiara Bartolozzi, Brian Taba, Andrea Censi, Stefan Leutenegger, Andrew Davison, Jörg Conradt, Kostas Daniilidis, and Davide Scaramuzza, "Event-based vision: A survey," *IEEE Trans. Pattern Anal. Mach. Intell.*, 2020. 2
- [15] Guillermo Gallego, Henri Rebecq, and Davide Scaramuzza, "A unifying contrast maximization framework for event cameras, with applications to motion, depth, and optical flow estimation," in *IEEE Conf. Comput. Vis. Pattern Recog. (CVPR)*, pp. 3867–3876, 2018. 2, 3, 4, 5
- [16] Arren Glover and Chiara Bartolozzi, "Event-driven ball detection and gaze fixation in clutter," in *IEEE/RSJ Int. Conf. Intell. Robot. Syst. (IROS)*, pp. 2203–2208, 2016. 2
- [17] Valentina Vasco, Arren Glover, Elias Mueggler, Davide Scaramuzza, Lorenzo Natale, and Chiara Bartolozzi, "Independent motion detection with event-driven cameras," in *IEEE Int. Conf. Adv. Robot. (ICAR)*, 2017. 2
- [18] Anton Mitrokhin, Cornelia Fermuller, Chethan Parameshwara, and Yiannis Aloimonos, "Event-based moving object detection and tracking," in *IEEE/RSJ Int. Conf. Intell. Robot. Syst. (IROS)*, 2018. 2, 3, 5, 6, 7
- [19] Timo Stoffregen and Lindsay Kleeman, "Simultaneous optical flow and segmentation (SOFAS) using Dynamic Vision Sensor," in *Australasian Conf. Robot. Autom. (ACRA)*, 2017. 2, 5, 6
- [20] Timo Stoffregen, Guillermo Gallego, Tom Drummond, Lindsay Kleeman, and Davide Scaramuzza, "Event-based motion segmentation by motion compensation," in *Int. Conf. Comput. Vis. (ICCV)*, pp. 7243–7252, 2019. 2, 3, 5, 6, 7, 8
- [21] Chethan M Parameshwara, Nitin J Sanket, Arjun Gupta, Cornelia Fermuller, and Yiannis Aloimonos, "MOMS with Events: Multi-object motion segmentation with monocular event cameras," *arXiv:2006.06158*, 2020. 2, 3, 5, 6, 7

- [22] Anton Mitrokhin, Chengxi Ye, Cornelia Fermuller, Yiannis Aloimonos, and Tobi Delbruck, “EV-IMO: Motion segmentation dataset and learning pipeline for event cameras,” in *IEEE/RSJ Int. Conf. Intell. Robot. Syst. (IROS)*, 2019. [2](#), [3](#), [5](#), [6](#), [7](#), [8](#)
- [23] John Winn and Jamie Shotton, “The layout consistent random field for recognizing and segmenting partially occluded objects,” in *IEEE Conf. Comput. Vis. Pattern Recog. (CVPR)*, vol. 1, pp. 37–44, 2006. [3](#)
- [24] Derek Hoiem, Carsten Rother, and John Winn, “3D LayoutCRF for multi-view object class recognition and segmentation,” in *IEEE Conf. Comput. Vis. Pattern Recog. (CVPR)*, pp. 1–8, 2007. [3](#)
- [25] Werner Trobin, Thomas Pock, Daniel Cremers, and Horst Bischof, “Continuous energy minimization via repeated binary fusion,” in *European conference on computer vision*, pp. 677–690, Springer, 2008. [3](#)
- [26] Stefan Roth, Victor Lempitsky, and Carsten Rother, “Discrete-continuous optimization for optical flow estimation,” in *Statistical and Geometrical Approaches to Visual Motion Analysis*, pp. 1–22, Springer, 2009. [3](#)
- [27] Jiaolong Yang and Hongdong Li, “Dense, accurate optical flow estimation with piecewise parametric model,” in *IEEE Conf. Comput. Vis. Pattern Recog. (CVPR)*, pp. 1019–1027, 2015. [3](#), [4](#)
- [28] Hossam Isack and Yuri Boykov, “Energy-based geometric multi-model fitting,” *International journal of computer vision*, vol. 97, no. 2, pp. 123–147, 2012. [3](#)
- [29] Yuri Boykov, Olga Veksler, and Ramin Zabih, “Fast approximate energy minimization via graph cuts,” *IEEE Trans. Pattern Anal. Mach. Intell.*, vol. 23, no. 11, pp. 1222–1239, 2001. [3](#), [4](#), [5](#)
- [30] Jonathan Richard Shewchuk, “General-dimensional constrained delaunay and constrained regular triangulations, i: Combinatorial properties,” in *Twentieth Anniversary Volume.*, pp. 1–58, Springer, 2009. [3](#)
- [31] Chris Russell, Joao Fayad, and Lourdes Agapito, “Energy based multiple model fitting for non-rigid structure from motion,” in *CVPR 2011*, pp. 3009–3016, IEEE, 2011. [3](#)
- [32] Guillermo Gallego, Mathias Gehrig, and Davide Scaramuzza, “Focus is all you need: Loss functions for event-based vision,” in *IEEE Conf. Comput. Vis. Pattern Recog. (CVPR)*, pp. 12272–12281, 2019. [3](#)
- [33] Rafael C Gonzalez, Richard Eugene Woods, and Steven L Eddins, *Digital image processing using MATLAB*. Pearson Education India, 2004. [3](#)
- [34] Guillermo Gallego and Davide Scaramuzza, “Accurate angular velocity estimation with an event camera,” *IEEE Robot. Autom. Lett.*, vol. 2, no. 2, pp. 632–639, 2017. [3](#)
- [35] Renfrey Burnard Potts, “Some generalized order-disorder transformations,” in *Mathematical proceedings of the cambridge philosophical society*, vol. 48, pp. 106–109, Cambridge University Press, 1952. [4](#)
- [36] Andrew Delong, Anton Osokin, Hossam N Isack, and Yuri Boykov, “Fast approximate energy minimization with label costs,” *Int. J. Comput. Vis.*, vol. 96, no. 1, pp. 1–27, 2012. [4](#), [5](#)
- [37] Mohammed Mutlaq Almatrafi, Raymond Baldwin, Kiyoharu Aizawa, and Keigo Hiraakawa, “Distance surface for event-based optical flow,” *IEEE Trans. Pattern Anal. Mach. Intell.*, 2020. [5](#), [6](#), [7](#), [8](#)
- [38] Nitin J. Sanket, Chethan M. Parameshwara, Chahat Deep Singh, Ashwin V. Kuruttukulam, Cornelia Fermüller, Davide Scaramuzza, and Yiannis Aloimonos, “EVDodgeNet: Deep dynamic obstacle dodging with event cameras,” in *IEEE Int. Conf. Robot. Autom. (ICRA)*, 2020. [7](#)
- [39] Christian Brandli, Raphael Berner, Minhao Yang, Shih-Chii Liu, and Tobi Delbruck, “A 240x180 130dB 3 μ s latency global shutter spatiotemporal vision sensor,” *IEEE J. Solid-State Circuits*, vol. 49, no. 10, pp. 2333–2341, 2014. [7](#), [8](#)
- [40] Min Liu and Tobi Delbruck, “Adaptive time-slice block-matching optical flow algorithm for dynamic vision sensors,” in *British Mach. Vis. Conf. (BMVC)*, 2018. [7](#)